Available online at www.sciencedirect.com
ScienceDirect
Sedimentary Geology 196 (2007) 269–277
Sedimentary Geology
www.elsevier.com/locate/sedgeo

AVA analysis reveals in situ sediment diagenesis at the Costa Rican décollement☆

Michael Schnabel [a,*], Ernst R. Flueh [a,b], Dirk Klaeschen [a,b], Matthias Zillmer [b]

[a] SFB 574, Christian-Albrechts-Universität Kiel, Wischhofstr. 1-3, 24148 Kiel, Germany
[b] IFM-GEOMAR, Leibniz-Institut für Meereswissenschaften, Wischhofstr. 1-3, 24148 Kiel, Germany

Abstract

Complete sediment subduction at the Costa Rica subduction zone makes this convergent margin an ideal place to investigate the effects of tectonic deformation in situ. We present a seismic reflection study along a line located 3 km landward of the Middle American Trench and oriented parallel to the strike of the décollement. The Ocean Bottom Hydrophone (OBH) seismic data include large offsets and incidence angles at the reflectors. We derive the P- and S-waves velocity distribution below the décollement using a P-wave analysis of amplitude with reflection angle. The investigation shows that there are unexpected large lateral velocity variations at a scale of only a few 100 m. The shear wave velocity in the uppermost subducted sediment varies between 300 and 700 m/s, while the variation of the compressional wave velocity is in a range of 1700 to 2000 m/s. The variation of the v_P–v_S ratio between 2.8 and 5.2 can only be explained by variations of the pore fluid pressure. The modelled velocities correspond to a normalised pore fluid pressure ratio λ^* in the range between 0.02 and 0.93. The most reasonable explanation for these observations is the localised presence of fluids, which are released during diagenesis by smectite to illite transformation. During this process, which takes place in three discrete steps, the interlayer water of the smectite is added to the pore fluid and the permeability of the sediment is decreased. Both effects lead to the formation of small, overpressured cells.

Keywords: Décollement; Costa Rica; Amplitude variation with offset; Pore pressure; Smectite; Diagenesis

1. Introduction

Convergent plate boundaries belong to the most active geologic environments on Earth. The diagenetic transformations of the sediments and the distribution of fluids and fluid sources are key factors for the understanding of subduction zones. These factors govern the geometric shape of the subduction zone (Davis et al., 1983), they lead to subduction erosion (von Huene et al., 2004), and affect the updip limit of the seismogenic zone (Moore and Saffer, 2001).

At the Costa Rican margin, nearly all oceanic sediment is subducted below the overriding plate (Moritz et al., 2000). Therefore, this margin is an ideal place to study processes affecting sediments during the transport from the seafloor to deeper parts of the subduction zone.

Up to now, the estimation of physical properties of subducted sediments off Costa Rica was based on information of ODP site 170 (e.g., Saffer et al., 2000; Gettemy and Tobin, 2003). This data is restricted to single points of the margin. In this study, we characterise the sediments along a strike profile of the décollement. By

☆ Sedimentary Geology special issue: Deformation of soft sediments in nature and laboratory, edited by Paola Vannucchi and Fabrizio Storti.

* Corresponding author. Now at: Federal Institute for Geosciences and Natural Resources, Stilleweg 2, 30655 Hannover, Germany. Tel.: +49 511 6432912.
E-mail address: michael.schnabel@bgr.de (M. Schnabel).

0037-0738/$ - see front matter © 2006 Elsevier B.V. All rights reserved.
doi:10.1016/j.sedgeo.2006.06.003

analysing the angle dependent amplitude of the reflected compressional wave, we are able to map the shear wave velocity (v_S) of the subducted sediment in addition to the compressional wave velocity (v_P). The combined use of v_P and v_S is a much better basis for the interpretation of the ongoing processes than using only v_P.

2. Regional setting

The Cocos Plate is subducted at a rate of 88 mm/yr beneath the Caribbean Plate at the Middle American Trench west of Costa Rica (Fig. 1). Offshore southern Costa Rica, the early Miocene oceanic crust is covered with 400 to 500 m of hemipelagic and pelagic sediments. Due to the erosive character of this margin, no accretion is taking place, and the oceanic sediment is fully subducted below the margin wedge (Moritz et al., 2000). This wedge has an age of at least 3 to 4 Ma (Morris et al., 2002) and is built entirely from material sourced from the landward sedimentary apron by debris flow and mass movements. The sediments within the wedge are fairly well compacted, while the younger subducted sedimentary section has a much higher porosity. At ODP site 1043 the overlying wedge has a porosity of 55%, compared to 70% in the underlying sediment. Further landward, at site 1040, the porosity is 42% in the wedge opposed to 58% below the décollement. The difference in age and physical properties leads to a pronounced reflection of negative polarity at the décollement (Shipley et al., 1990). According to Tobin et al. (2001), the décollement zone comprises the lowermost 9 m of the overriding wedge at site 1043, while at site 1040 this zone shows a thickness of 38 m. An inversion of density logs has lead to the result that this boundary is characterised by a sharp discontinuity of the P-wave velocity (McIntosh and Sen, 2000). This means that in the vicinity of ODP leg 170, the plate boundary is a discontinuity of first order. An effective dewatering with ongoing subduction can be inferred from the observed changes in the thickness of underthrust sediments as they are progressively buried beneath the margin wedge (Saffer et al., 2000). The lowermost part of the overlying wedge is characterised by effective shear-enhanced compaction (Kopf et al., 2000). This layer acts as a seal which inhibits a vertical fluid flow out of the subducted sediment. This interpretation is supported by the lack of localised fluid expulsion at the seafloor in the frontal part of the subduction zone (Kahn et al., 1996).

We have chosen to investigate a region offshore southern Costa Rica, between the Quepos Plateau and the Cocos Ridge, where the décollement shows the brightest reflection compared to the rest of the margin (Hinz et al., 1996). Parallel to the trench, the zero-offset amplitude of the décollement reflection varies on the order of 200%. This paper focuses on this exceptional area.

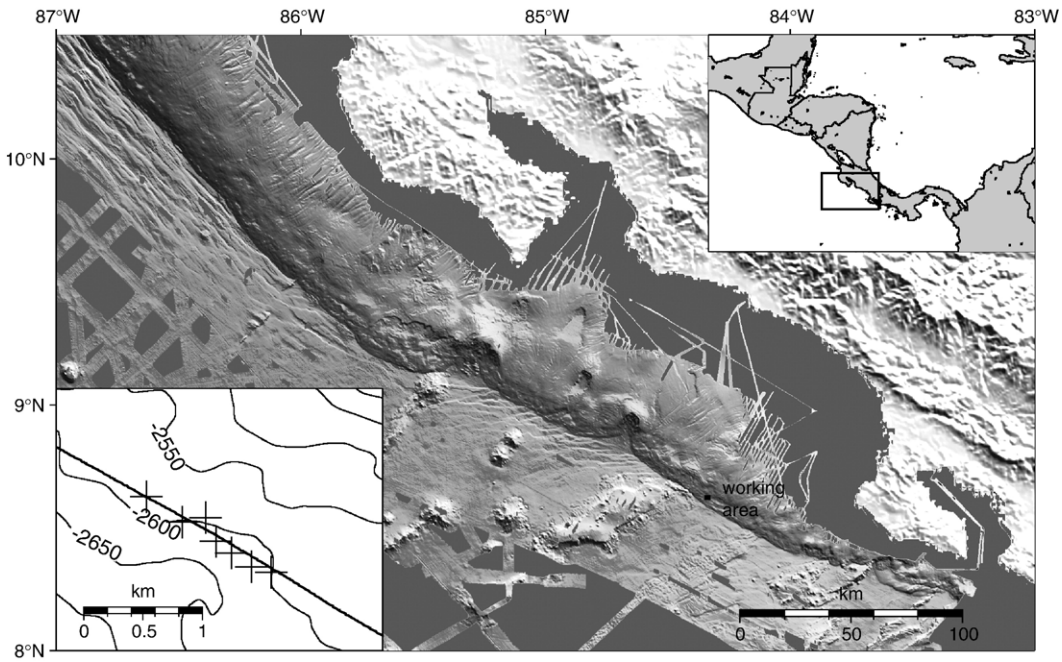

Fig. 1. Regional setting of the working area. The map shows the Middle American Trench offshore Costa Rica. In the upper right image, an overview of the Middle American Landbridge can be seen. In the lower left box, the positions of the ocean bottom hydrophones and of the seismic line are displayed. All instruments lie near the 2600 m isoline.

3. Seismic dataset and method of investigation

In this study we analyse the recordings of seven Ocean Bottom Hydrophones (OBH), which were deployed during RV Sonne cruise SO173 in summer 2003. As seismic source we used a 1.7 l GI gun (frequencies up to 150 Hz) with a shot interval of about 10 m and a 32 l Bolt gun (frequencies between 5 to 10 Hz) with a shot interval of nearly 60 m. The stations were positioned along profile 34 at the sea floor in 2600 m depth below the sea level at an average spacing of 200 m. Reflections from the décollement were recorded at all stations for offsets up to 3500 m. At greater offsets the décollement reflection was distorted by the arrival of the direct wave.

To avoid any artifacts, the seismic data processing is kept to a minimum and restricted to a high pass filter. Peak-to-peak amplitudes for the reflection of the décollement are picked for each single trace of the record sections. This results in about 600 amplitude values for each station. These amplitudes are corrected for the spherical divergence and for the source directivity of the air-gun (Zillmer et al., 2005). The comparison of the seafloor reflection with its multiple in the water column gives the seafloor reflection coefficient (Warner, 1990). The obtained reflection coefficient of 0.20 is used to calibrate the décollement amplitudes. In this way true reflection coefficients for the selected horizons are obtained.

To estimate the P-wave velocity-depth profile in the sedimentary wedge, we use the reflection traveltime hyperbolas, which were recorded on four different strike profiles. On all profiles the velocity-depth gradient is in the range between 0.75 to 0.80 s^{-1}, independent of the distance to the trench. To derive a second velocity estimate, we apply Kirchhoff depth migration to the seismogram sections (Fig. 2). This method delivers a 1-D velocity model for each section. For all stations, the imaging of the BSR at 140 m below seafloor (mbsf) yields a velocity of 1550 m/s within the uppermost sediments, while the décollement is best imaged with a velocity of 2100 m/s at the base of the sedimentary wedge. Therefore, we can conclude that the velocity disribution down to the décollement is constant along the profile. The resulting velocities are in good agreement with global means for terrigeneous sediments: Hamilton (1979) reported a velocity of 2150 m/s at the corresponding depth of 700 mbsf.

Since the water depth along this profile varies in a range of less than 2%, we use the resulting migration velocities to construct an average velocity model for the whole profile. Based on this model, we perform ray tracing to determine the ray path in the subsurface. This leads to the position of the reflection points at the décollement and to the incident angles of the seismic waves at this boundary. We combine this geometric information with the amplitude values at each trace for each shot. The reflecting horizon was divided in 10 m wide intervals. For each interval, we obtain values from 4 or 5 shots and from 5 or 6 different hydrophones (which corresponds to different reflection angles). Two examples for this data are shown in Fig. 3.

Comparing the corrected amplitudes from the GI gun seismogram sections with the amplitudes from the Bolt gun sections shows that the reflection coefficient is frequency independent. In conclusion the reflector is a first order discontinuity.

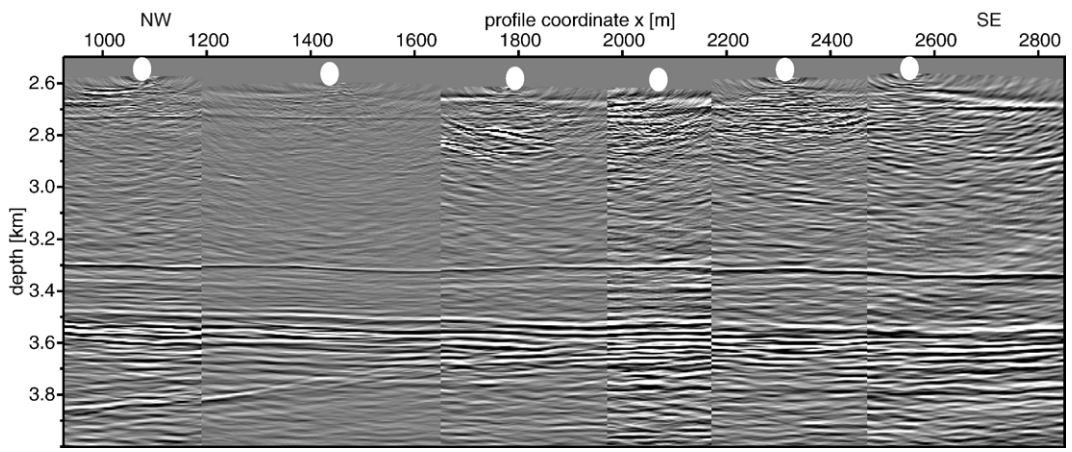

Fig. 2. Depth migration of the selected profile. For this image, data of six OBH were combined. The positions of the hydrophones at the seafloor in 2600 m water depth are shown as white ellipses. The décollement is imaged at 3300 m below sea level (bsl) and the top of the oceanic crust at 3500 mbsl.

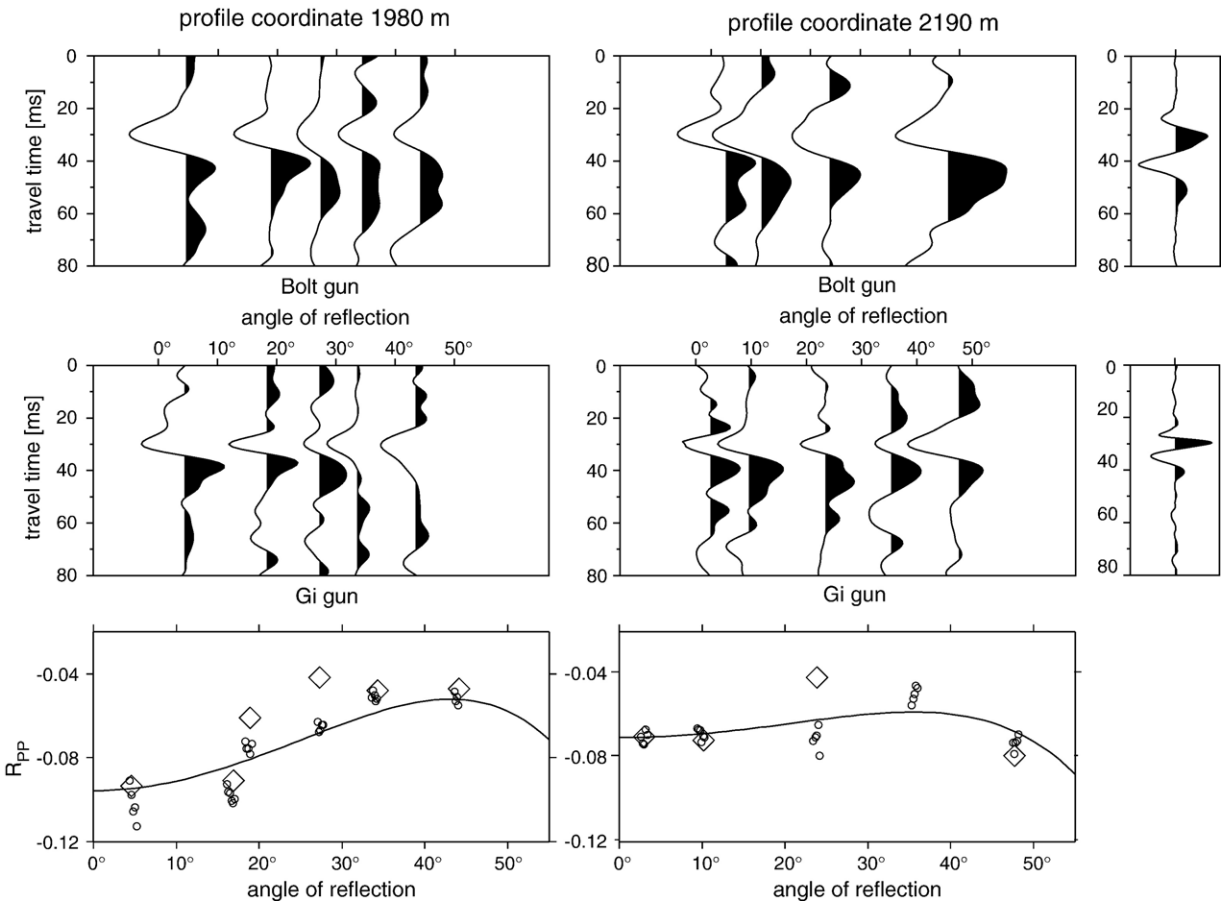

Fig. 3. Data examples for two points of the profile. At the seismic traces, the reflection of the décollement is shifted to 30 ms. Each trace was recorded at a different OBH. The waveforms for both seismic sources are comparable. For comparison, the source wavelets are shown on the right hand side. In the lower row, the measured reflection coefficients for the Bolt gun (diamonds), for the GI gun (circles), and the modelled P-wave reflection coefficient (solid line) are shown. At profile coordinate $x=1980$ m low velocities in the subducted sediment are needed to explain the reflection coefficient curve ($v_P=1750$ m/s and $v_S=320$ m/s). The example at profile coordinate 2190 m shows higher velocities below the décollement ($v_P=1850$ m/s and $v_S=550$ m/s).

The angle dependence of the P-wave reflection coefficient $R_{PP}(\theta)$ is described by the Zoeppritz equations (e.g., Aki and Richards, 1980). These equations give the reflection coefficient for plane waves as a function of six independent elastic parameters, three for each medium on both sides of the interface. The parameters are the P- and S-wave velocities and the density ρ. Shuey (1985) derived a simplification of these equations. His approximation consists of three terms, where each term describes a different range of reflection angles. For the zero offset case, the reflection coefficient is determined by the relative change in v_P and ρ. At intermediate angles up to 30° the amplitude depends mainly on the difference in the Poisson's ratio across the interface. At larger angles the coefficient is determined by the change in v_P. Since our data set comprises reflections for angles greater than 30°, we are able to describe three independent parameters.

We set the three parameters in the overlying wedge above the décollement to fixed values for the whole profile. This assumption is supported by the lateral homogeneous velocity distribution which resulted from the depth migration. Further support comes from recent sidescan sonar imaging of the seafloor, which did not show any anomalous structures such as mounds which are related to fluid escape in this area (Flueh et al., 2004). The P-wave velocity above the décollement was set to 2100 m/s. This value is the result of the depth migration and is confirmed by ray tracing. The S-wave velocity was set to 730 m/s, according to Hamilton's (1976) formula:

$$v_S = 0.58d + 322, \quad (1)$$

where d denotes the depth below sea floor, measured in metres. The density–velocity relationship of Gardner et al. (1974):

$$\rho = 0.31\ v_P^{0.25}, \quad (2)$$

where ρ is the density measured in g/cm^3, results in a density of 2.1 g/cm^3 above the plate boundary. These values for v_S and ρ are in good agreement with measurements of ODP Leg 170 at the Costa Rican margin (Kimura et al., 1997). Bangs et al. (2004) have also shown by a 3 D amplitude analysis at the Nankai Trough that the amplitude variations at the plate boundary cannot be attributed to changes in the overlying wedge.

We calculate the angle dependent reflection coefficient at the plate boundary. By varying the elastic parameters of the underlying sediment, we try to fit this reflection curve to the measured amplitude values for each 10 m wide interval of our profile. Two examples for such curves are shown in the lower part of Fig. 3.

4. Results

The modelling described in Section 3 results in velocity and density distributions for the subducted sediment directly below the décollement. The density below the décollement is constant along the whole profile at about 2.0 g/cm^3. The resulting velocities are displayed in Fig. 4. The P-wave velocity varies between 1700 and 2000 m/s. For the S-wave velocity, values between 300 and 700 m/s are obtained. While v_P varies only by 15%, v_S varies by more than 50%, and the v_P–v_S ratio reaches values as high as 5 for some reflection points along the profile.

According to Mavko et al. (1998), the v_P–v_S relationship for a broad range of water saturated shaley sands can be described by the following formula (velocities given in km/s):

$$v_S = 0.794\ v_P - 0.787. \quad (3)$$

We estimated the shear velocity based on this equation. The result is plotted in Fig. 4 (solid line) for comparison. In areas where v_P is near 2000 m/s, Eq. (3) is able to predict v_S, while in areas with v_P near 1800 m/s the S-wave velocity is overestimated by nearly 100%. This implies that the large variation in v_S cannot be explained by variations in clay content or porosity. We suggest that the velocity variation along the profile is caused by variations of the pore pressure.

The effective pressure P_{eff} is given by the difference of the lithostatic pressure P_L and the pore pressure P_P. A decrease of the effective pressure in water saturated sediments causes both P-wave velocity and S-wave velocity to decrease, but the greater effect on v_S causes an increase in v_P–v_S ratio (Nur, 1972). For the extreme case that the pore pressure is close to the lithostatic pressure, an unconsolidated sediment will behave like a suspension. Since P-wave velocity in a suspension is close to that of the suspending fluid and S-waves cannot propagate in suspensions, the v_P–v_S ratio must dramatically increase as P_{eff} approaches zero (Mukerji et al., 2002). Zimmer

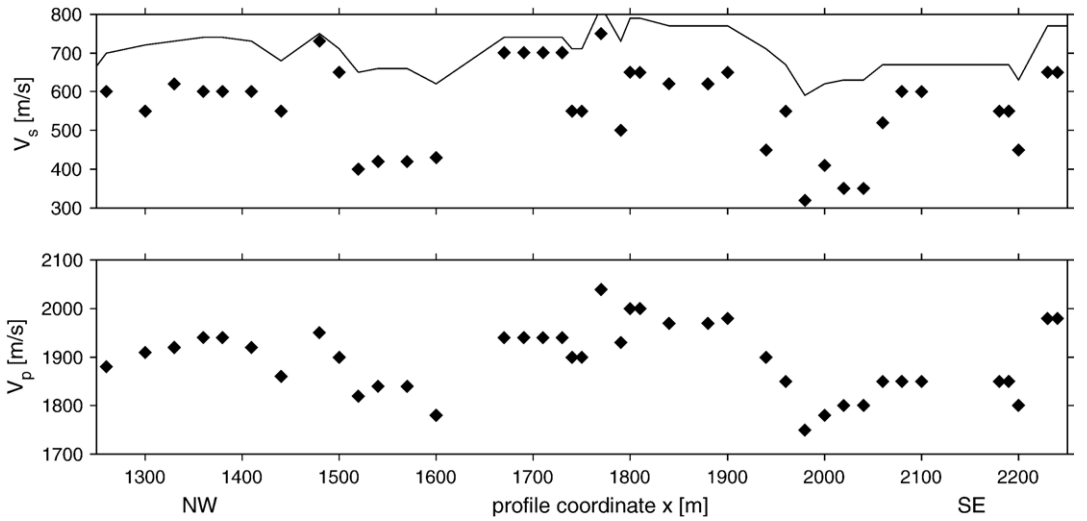

Fig. 4. Modelled velocities for the sediment below the décollement. The solid line represents the expected v_S for a broad range of water saturated shaley sands (Mavko et al., 1998). In areas with a low P-wave velocity, the measured S-wave velocity is lower than expected.

(2003) conducted laboratory measurements on unconsolidated sediments and he found a v_P–v_S ratio of as high as 9.8 for an effective pressure of 0.15 MPa. Previous research at different subduction zones has also shown that a varying fluid pressure is the most likely property change that can affect the impedance so strongly (Shipley et al., 1994; Tobin et al., 1994; Moore et al., 1995).

With laboratory measurements of the relationship between v_S and P_{eff}, and from estimates of the hydrostatic pressure P_H and the lithostatic pressure P_L, we can derive the normalised pore pressure ratio to describe fluid pressures in situ. Therefore, we use measurements which were conducted with coarse sands (Prasad, 1988) and fine sands (Zimmer, 2003) with grain sizes between 82 μm and 134 μm and initial porosities between 39.7% and 42.7%. Zimmer (2003) was able to measure shear velocities for effective pressures as low as 0.1 MPa. Zimmer et al. (2002) have shown that v_S is much more affected by a change in P_{eff} than v_P. Therefore, we use only the S-wave velocity to estimate the effective pressure. In both experiments the S-wave velocity obeys the following equation:

$$v_S = 1.8\ P_{eff}^{0.26}. \quad (4)$$

ODP leg 170 has shown that the uppermost subducted sediment can be described as silty clay with silty sand interbeds (Kimura et al., 1997). Extrapolation of porosity from site 1043 (0.6 km landward of the trench) and site 1040 (1.7 km landward of the trench) leads to a porosity estimate between 40% and 45% for our profile. Unfortunately, no laboratory data is available for this specific lithology. On the other hand, Prasad (2002) has shown that the pressure dependence of seismic velocities in unconsolidated sand forms a uniform trend for a large range of grain sizes. Therefore, we use Eq. (4) to calculate the effective pressure below the décollement. We adopt the seafloor as a reference level (Davis et al., 1983) and determine the hydrostatic pressure P_H and the lithostatic pressure P_L at 700 mbsf. With these values, we are able to determine the normalised pore pressure ratio

$$\lambda^* = (P_L - P_{eff} - P_H)/(P_L - P_H). \quad (5)$$

The results are shown in Fig. 5.

In areas with a low S-wave velocity (profile coordinates 1550 m and 2000 m) the effective pressure below the décollement is lower than 1 MPa. This corresponds to a normalised pore pressure ratio λ^* of up to 0.93. In areas with a higher v_S (i.e. where v_S is near the predicted curve in Fig. 4, near 1500 m and 1800 m of the profile) P_{eff} is in the range of 6 to 7 MPa. At these points, λ^* is lower than 0.1.

The S-wave velocity within the overlying wedge was determined by a global average (Eq. (1)). To investigate the effects of this value, we vary it by 100 m/s and model again the parameters for the underlying sediment. The resulting changes for the S-wave velocities are on the same order, but the relative differences along the profile are not affected. The differences in the v_P–v_S ratio are still on an order which can only be explained by variations in the pore pressure. A varying density in the overlying wedge has no effect on the seismic velocities below the décollement. Finally, we estimate the absolute error of our modelling. We are able to determine the velocities with an error smaller than 50 m/s. Even for the worst case, v_S varies along our profile between 350 m/s and 650 m/s, which corresponds to a normalised pore pressure ratio between 0.07 and 0.91.

5. Discussion

Large lateral variations of pore pressure are an unexpected result. In this section, we discuss which factors might influence the fluid pressure in a subduction zone.

During subduction, the oceanic sediments are progressively loaded and heated as they are thrust under the

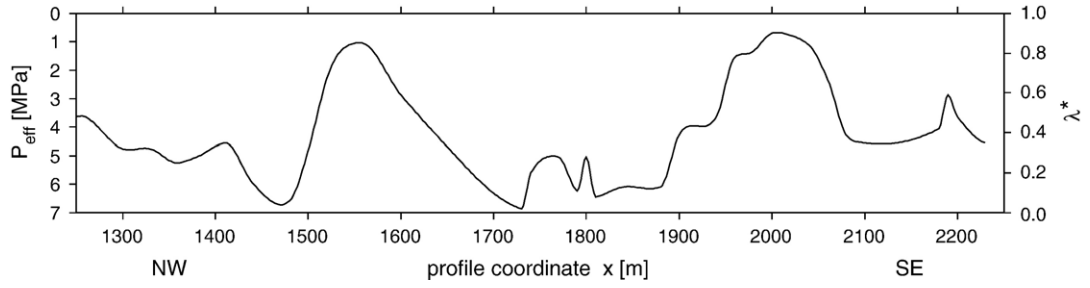

Fig. 5. Resulting effective pressure P_{eff} and normalised pore pressure ratio within the subducting sediment. The pressure ranges from near hydrostatic (between 1700 m and 1900 m) to near lithostatic (at 1550 m and at 2000 m).

margin wedge. The additional overburden stress is transferred to the pore fluid. In the case of high permeability the excess pore pressure causes dewatering and the hydrostatic pore pressure is maintained. In the case of low permeability or a high subduction velocity, this dewatering cannot keep pace with the increase in overburden stress. This results in an increase of excess pore pressure (P_P–P_H) with ongoing subduction. This process belongs to the static model for hydrodynamic phenomena (Neuzil, 1995): abnormal pressures can be viewed as relict features preserved by a virtual absence of fluid flow over geologic time.

Saffer (2003) discussed a vertically varying permeability of the décollement based on observations of different dewatering at two drill holes of ODP 170. In areas of a high-permeability décollement, a vertical fluid flow into the margin wedge is allowed, while in areas of a low-permeability décollement, fluids are trapped below the interface. This explanation for the lateral variation in the pore pressure is not in accordance with geochemical analyses of the fluids in the subduction zone. Kopf et al. (2000) have shown that the fluids below and above the décollement have quite different signatures, which is not in accordance with a significant fluid transfer across the plate boundary. Saffer and McKiernan (2005) estimated the dewatering to be extremely rapid at the Costa Rican margin (8 m^3 yr^{-1} m^{-1} of margin length). A fluid flux of this order does not allow the building of overpressures as high as $\lambda^*=0.93$ by static processes alone. The efficient dewatering within our area of investigation is also supported by the steep taper ($\beta=8.6°$) of the sedimentary wedge (Saffer and Bekins, 2002). For the same reasons, the explanation of the observed pattern by a lateral variation of horizontal permeability within the subducted sediment can be ruled out.

The décollement zone is generally a major pathway for fluids from deeper parts of the subduction zone (Silver et al., 2000). The analysis of lithium concentration and isotopic ratios has shown that these fluids originated from mineral fluid dehydration and transformation reactions at temperatures up to 150 °C (Chan and Kastner, 2000). Brown et al. (1994) have shown that this flow along the plate boundary can only take place within heterogeneous open fracture systems. Fitts and Brown (1999) provided geochemical evidence for these finger-like flow paths at the Barbados décollement.

A lateral channelled heterogeneous fluid flow as described above would not explain the observed variability in the décollement reflection. At the Costa Rican margin, these fluids are travelling within the upper, brittle domain of the décollement zone (Tobin et al., 2001). The dominant seismic reflector is the lower boundary of the décollement (McIntosh and Sen, 2000), where the P-wave velocity forms a discontinuity of first order (Fig. 6). Varying velocities within the several metres thick décollement zone would lead to interference within the reflected wave, which is not observed in the recorded data. Even if the fluids from the deeper part of the subduction zone are travelling along finger-like channels, this phenomenon is not visible on a seismic scale. Therefore, the reasons for the variations of the reflection amplitude must be due to processes below the plate boundary.

According to Neuzil (1995), areas of overpressuring can also be caused by hydrodynamic phenomena such as compaction, diagenesis, or deformation. These processes can act as distributed fluid sources or sinks. One of these diagenetic reactions is the smectite to illite transformation (Powers, 1967). Within our study area, the subducted hemipelagic sediment contains 60 wt.% of smectite (Spinelli and Underwood, 2004). The smectite dehydration takes places in three separate steps (Colton-Bradley, 1987). The first step occurs at about 60 °C and causes an overall increase in volume of 1.4% due to the expansion of interlayer water (Osborne and Swarbrick, 1997). Measurements of the geothermal gradient offshore southern Costa Rica shows that the temperature along the investigated profile is near 60 °C (Soeding et al., 2003), which means that the conditions for the onset of smectite dehydration are reached at a depth of 700 m below the seafloor. The relationship

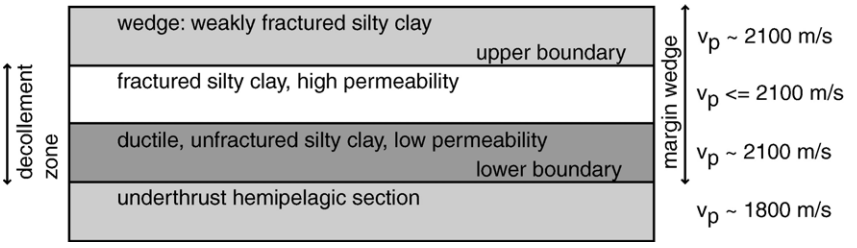

Fig. 6. Décollement domain, modified after Tobin et al. (2001). Based on drilling results, the décollement zone comprises the lowermost part of the overlying wedge. The main impedance contrast is the lower boundary of the décollement zone.

between a relative change in volume $\Delta V/V$ and the resulting change in the pore pressure ΔP_P is:

$$\Delta P_P = \kappa \Delta V/V. \quad (6)$$

The bulk modulus κ of the pore fluid is about 2.8 GPa (Batzle and Wang, 1992). We use this relation to show that a relative volume change on the order of 0.25% due to the release of bounded water is sufficient to cause a change in the pore pressure of about 7 MPa. This change corresponds to the difference between the hydrostatic and the lithostatic pressure along the investigated profile and would be able to explain the measured variability in λ^* between 0.02 and 0.93. Bethke (1986) has shown that the smectite dehydration reaction can lower the permeability of the sediment by an order of two magnitudes. This process traps the fresh fluid within small, overpressured cells.

6. Summary

By analysing the amplitudes for near and far offset reflections, we have mapped the velocity distribution along strike at the décollement in our area of investigation. We found moderate variations of v_P (up to 15%) directly below the décollement. The variations of v_S are much more pronounced in the order of 50%. They are explained by differences in the pore pressure within the subducted sediment. A comparison to laboratory data on soft sediments shows that these velocity variations correspond to variations of the normalised pore pressure λ^* between 0.02 and 0.93. The only feasible explanation for pressure cells of this order is a localised dewatering of the subducting smectite.

Acknowledgements

The manuscript benefited from instructive reviews of N. Bangs and an anonymous reviewer. This work was supported by the Sonderforschungsbereich 574 at Kiel University (publication number 88 of the SFB 574).

References

Aki, K.I., Richards, P.G., 1980. Quantitative seismology: theory and methods. W.H. Freeman and Co, San Fransico.

Bangs, N.L., Shipley, T.H., Gulick, T.H., Moore, G.F., Kuromoto, S., Nakamura, Y., 2004. Evolution of the Nankai Trough décollement from the trench into the seismogenic zone: inferences from three-dimensional seismic reflection imaging. Geology 32, 273–276, doi:10.1130/G20211.1.

Batzle, M., Wang, Z., 1992. Seismic properties of pore fluids. Geophysics 57, 1396–1408.

Bethke, C.M., 1986. Inverse hydrologic analysis of the distribution and origin of Gulf Coast-type geopressured zones. J. Geophys. Res. 91, 6535–6545.

Brown, K.M., Bekins, B., Clennell, B., Dewhurst, D., Westbrook, G., 1994. Heterogeneous hydrofracture development and accretionary fault dynamics. Geology 22, 259–262.

Chan, L.-H., Kastner, M., 2000. Lithium isotopic compositions of pore fluids and sediments in the Costa Rica subduction zone: implications for fluid processes and sediment contribution to the arc volcanoes. Earth Planet. Sci. Lett. 183, 275–290.

Colton-Bradley, V.A., 1987. Role of pressure in smectite dehydration — effects on geopressure and smectite-to-illite transformation. AAPG Bull. 71, 1414–1427.

Davis, D., Suppe, J., Dahlen, F.A., 1983. Mechanics of fold- and thrust belts and accretionary wedges. J. Geophys. Res. 88, 1153–1172.

Fitts, T.G., Brown, K.M., 1999. Stress-induced smectite dehydration: ramifications for patterns of freshening and fluid expulsion in the N. Barbados accretionary wedge. Earth. Planet. Sci. Lett. 172, 179–197.

Flueh, E.R., Soeding, E., Suess, E., 2004. RV Sonne cruise report SO173/1,3&4. GEOMAR Report, vol. 115. 491 pp.

Gardner, G.H.F., Gardner, L.W., Gregory, A.R., 1974. Formation velocity and density — the diagnostic basis for stratigraphic traps. Geophysics 39, 770–780.

Gettemy, G.L., Tobin, H.J., 2003. Tectonic signatures in centimeter-scale velocity–porosity relationships of Costa Rica convergent margin sediments. J. Geophys. Res. 108 (B10), 2494, doi:10.1029/2001JB000738.

Hamilton, E.L., 1976. Shear-wave velocity versus depth in marine sediments: a review. Geophysics 41, 985–996.

Hamilton, E.L., 1979. v_P/v_S and Poisson's ratios in marine sediments and rocks. J. Acoust. Soc. Am. 66, 1093–1101.

Hinz, K., von Huene, R., Ranero, C.R., 1996. PACOMAR Working Group. Tectonic structure of the convergent Pacific margin offshore Costa Rica from multichannel seismic reflection data. Tectonics 15, 54–66.

Kahn, L.M., Silver, E.A., Orange, D., Kochevar, R., McAdoo, B., 1996. Surficial evidence of fluid expulsion from the Costa Rica accretionary prism. Geophys. Res. Lett. 23, 887–890.

Kimura, G., Silver, E., Blum, P., 1997. Proceedings of the ocean drilling program. Initial Reports, vol. 170. Ocean Drilling Program, College Station, Texas.

Kopf, A., Dehyle, A., Zuleger, E., 2000. Evidence for deep fluid circulation and gas hydrate dissociation using boron and boron isotopes of pore fluids in forearc sediments from Costa Rica (ODP Leg 170). Mar. Geol. 167, 1–28.

Mavko, G., Mukerji, T., Dvorkin, J., 1998. The rock physics handbook. Cambridge university press, Cambridge.

McIntosh, K.D., Sen, M.K., 2000. Geophysical evidence for dewatering and deformation processes in the ODP Leg 170 area offshore Costa Rica. Earth Planet. Sci. Lett. 178, 125–138.

Moore, J.C., Saffer, D., 2001. Updip limit of the seismogenic zone beneath the accretionary prism of southwest Japan: an effect of diagenetic to low-grade metamorphic processes and increasing effective stress. Geology 29, 183–186.

Moore, J.C., Moore, G.F., Cochrane, G.R., Tobin, H.J., 1995. Negative-polarity seismic reflections along faults of the Oregon accretionary prism: indicators of overpressuring. J. Geophys. Res. 100, 12895–12906.

Moritz, E., Bornholdt, S., Westphal, H., Meschede, M., 2000. Neural network interpretation of LWD data (ODP Leg 170) confirms complete sediment subduction at the Coast Rica convergent margin. Earth. Planet. Sci. Lett. 174, 301–312.

Morris, J.D., Valentine, R., Harrison, T., 2002. ^{10}Be imaging of sediment accretion and subduction along the northeast Japan and Costa Rica convergent margin. Geology 30, 59–62.

Mukerji, T., Dutta, N., Prasad, M., Dvorkin, J., 2002. Seismic detection and estimation of overpressures, part 1: the rock physics basis. CSEG Rec. 27, 36–57.

Neuzil, C.A., 1995. Abnormal pressures as hydrodynamic phenomena. Am. J. Sci. 295, 742–786.

Nur, A., 1972. Dilatancy, pore fluids, and premonitory variations of t_S/t_P travel times. Bull. Seismol. Soc. Am. 62, 1217–1222.

Osborne, M.J., Swarbrick, R.E., 1997. Mechanisms for generating overpressure in sedimentary basins: a reevaluation. AAPG Bull. 81, 1023–1041.

Powers, M.C., 1967. Fluid-release mechanisms in compacting marine mudrocks and their importance in oil exploration. AAPG Bull. 51, 1240–1254.

Prasad, M., 1988. Experimental and theoretical considerations of velocity and attenuation interactions with physical parameters in sand. Ph.D. thesis, Kiel University.

Prasad, M., 2002. Acoustic measurements in unconsolidated sands at low effective pressure and overpressure detection. Geophysics 67, 405–412.

Saffer, D.M., 2003. Pore pressure development and progressive dewatering in underthrust sediments at the Costa Rican subduction margin: comparison with northern Barbados and Nankai. J. Geophys. Res. 108 (B5), 2261, doi:10.1029/2002JB001787.

Saffer, D.M., Bekins, B.A., 2002. Hydrologic controls on the morphology and mechanics of accretionary wedges. Geology 30, 271–274.

Saffer, D.M., McKiernan, A.W., 2005. Permeability of underthrust sediments at the Costa Rican subduction zone: scale dependence and implications for dewatering. Geophys. Res. Lett. 32, L02302, doi:10.1029/2004GL021388.

Saffer, D.M., Silver, E.A., Fisher, A.T., Tobin, H., Moran, K., 2000. Inferred pore pressures at the Costa Rica subduction zone: implications for dewatering processes. Earth Planet. Sci. Lett. 177, 193–207.

Shipley, T.H., Stoffa, P.L., Dean, D.F., 1990. Underthrust sediments, fluid migration paths, and mud volcanoes associated with the accretionary wedge off Costa Rica: Middle America Trench. J. Geophys. Res. 95, 8743–8752.

Shipley, T.H., Moore, G.F., Bangs, N.L., Moore, J.C., Stoffa, P.L., 1994. Seismically inferred dilatancy distribution, northern Barbados Ridge décollement: implications for fluid migration and fault strength. Geology 22, 411–414.

Shuey, R.T., 1985. A simplification of the Zoeppritz equations. Geophysics 50, 609–614.

Silver, E., Kastner, M., Fisher, A., Morris, J., McIntosh, K., Saffer, D., 2000. Fluid flow paths in the Middle America Trench and Costa Rica margin. Geology 28, 679–682.

Soeding, E., Wallmann, K., Suess, E., Flueh, E., 2003. RV Meteor, cruise report M54/2-3: Caldera-Curacao. GEOMAR Report, vol. 111. 366 pp.

Spinelli, G.A., Underwood, M.B., 2004. Character of sediments entering the Costa Rica subduction zone: implications for partitioning of water along the plate interface. The Isl. Arc 13, 432–451, doi:10.1111/j.1440-1738.2004.00436.x.

Tobin, H.J., Moore, J.C., Moore, G.F., 1994. Fluid pressure in the frontal thrust of the Oregon accretionary prism: experimental constraints. Geology 22, 979–982.

Tobin, H.J., Vannucchi, P., Meschede, M., 2001. Structure, inferred mechanical properties, and implications for fluid transport in the décollement zone, Costa Rica convergent margin. Geology 29, 907–910.

von Huene, R., Ranero, C.R., Vannucchi, P., 2004. Generic model of subduction erosion. Geology 32, 913–916, doi:10.1130/G20563.1.

Warner, M., 1990. Absolute reflection coefficients from deep seismic reflections. Tectonophysics 173, 15–23.

Zillmer, M., Flueh, E.R., Petersen, J., 2005. Seismic investigation of a bottom simulating reflector and quantification of gas hydrate in the Black Sea. Geophys. J. Int. 161, 662–678, doi:10.1111/j.1365-246x.2005.02635.x.

Zimmer, M., 2003. Seismic velocities in unconsolidated sands: measurements of pressure, sorting, and compaction effects. Ph.D. thesis, Stanford University.

Zimmer, M., Prasad, M., Mavko, G., 2002. Pressure and porosity influences on v_P–v_S ratio in unconsolidated sands. The Lead. Edge 21, 178–183.